NANO LETTERS

Letter

pubs.acs.org/NanoLett

Highly Luminescent (Zn,Cd)Te/CdSe Colloidal Heteronanowires with Tunable Electron–Hole Overlap

Esther Groeneveld,*[,†] Susanne van Berkum,[†] Matti M. van Schooneveld,[‡] Alexandre Gloter,[§] Johannes D. Meeldijk,[∥] Dave J. van den Heuvel,[§] Hans C. Gerritsen,[§] and Celso de Mello Donega*[,†]

[†]Condensed Matter and Interfaces, Debye Institute, Utrecht University, 3508 TA Utrecht, Netherlands

[‡]Inorganic Chemistry & Catalysis, Debye Institute, Utrecht University, 3584 CA Utrecht, Netherlands

[§]Laboratoire de Physique des Solides, CNRS UMR 8502, Université Paris Sud XI, F 91405 Orsay, France

[∥]Electron Microscopy Utrecht, Utrecht University, 3584 CH Utrecht, Netherlands

[§]Molecular Biophysics, Debye Institute, Utrecht University, 3508 TA Utrecht, Netherlands

S *Supporting Information*

ABSTRACT: We report the synthesis of ultranarrow (Zn,Cd)Te/CdSe colloidal heteronanowires, using ZnTe magic size clusters as seeds. The wire formation starts with a partial Zn for Cd cation exchange, followed by self-organization into segmented heteronanowires. Further growth occurs by inclusion of CdSe. The heteronanowires emit in the 530 to 760 nm range with high quantum yields. The electron–hole overlap decreases with increasing CdSe volume fraction, allowing the optical properties to be controlled by adjusting the heteronanowire composition.

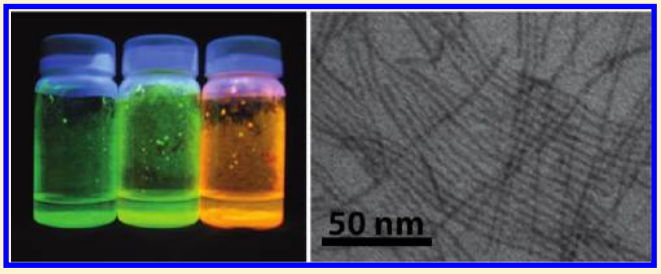

KEYWORDS: *Colloidal heteronanowire, photoluminescence, indirect exciton, electron–hole overlap, ZnTe–CdTe–CdSe*

An essential feature of colloidal semiconductor nanocrystals (NCs) is that nanoscale size effects can be fully exploited to engineer the material properties without changing its composition. Semiconductor NCs comprising two (or more) different materials joined together by heterointerfaces, that is, heteronanocrystals (HNCs), offer even more exciting possibilities regarding property control.[1] The localization regime of photoexcited charge carriers in HNCs (*viz.*, type-I, type-I$^{1/2}$, and type-II) is determined by the offsets between the energy levels of the materials that are combined at the heterointerface.[1] In the type-I regime (enclosed alignment), both charge carriers are localized in the same material, whereas in the type-II regime (staggered alignment) the electron and hole are primarily localized in different materials, that is, in different segments of the HNC. This spatial separation of the electron and hole wave functions leads to the formation of a spatially indirect exciton. In the type-I$^{1/2}$ (or quasi-type-II) regime, the offsets are such that one carrier is localized in one of the HNC components while the other is delocalized over the HNC.[1]

Since the energy levels of semiconductor NCs are strongly size- and shape-dependent, the energy offsets in HNCs can be tuned by controlling the composition, size, and shape of each component. This allows the electron–hole spatial overlap to be tailored, leading to a remarkable degree of control over the properties of nanoscale excitons in colloidal HNCs.[1−5] For example, the rates for Auger recombination,[6] hot carrier relaxation,[4] and spin relaxation[5] have been observed to decrease as a result of the (partial) spatial separation of the photoexcited carriers. Further, control over the electron–hole overlap in type-II (and type-I$^{1/2}$) HNCs has been used to tune the exciton radiative lifetimes,[3,6−8] the emission energies,[1,3,5,7,9] and the Stokes shifts[7] of colloidal semiconductor HNCs. This flexibility in tailoring the properties of HNCs has important consequences for a number of potential applications (for example, low-threshold lasers, photovoltaic devices, solar energy conversion, optical switches, LEDs, biomedical imaging, and so forth)[1] and has attracted increasing attention, leading to the investigation of a number of compositions, such as CdTe/CdSe,[6,7,9−15] CdSe/ZnTe,[9,16,17] ZnTe/ZnSe,[18] ZnSe/CdS,[3,4,19,20] ZnTe/CdS,[20] and CdSe/CdS.[21,22]

ZnTe/CdSe is a promising semiconductor combination for type-II HNCs, because the energy offsets between the valence and conduction bands are rather large (viz., 0.68 and 1.24 eV, respectively, for the bulk materials[23]). These large energy offsets facilitate the formation of spatially indirect excitons and should result in a wide tunability window for the electron–hole overlap in ZnTe/CdSe HNCs. In addition, the lattice mismatch between these two materials is small (0.8%).[24,25] ZnTe/CdSe heteronanostructures have been grown both by vapor phase epitaxial (VPE) deposition[26] and colloidal synthetic methods.[16−18] Despite the advantages of colloidal chemistry methods,[1] the development of ZnTe-based colloidal HNCs

Received: October 20, 2011
Revised: December 9, 2011
Published: January 3, 2012

dx.doi.org/10.1021/nl203695m | *Nano Lett.* 2012, 12, 749–757

has been slow, possibly hampered by the limited availability of high quality ZnTe NCs. Tetrapod shaped[17] and concentric nearly spherical[16] colloidal ZnTe/CdSe core/shell HNCs have been made, but the observed photoluminescence (PL) quantum yields (QYs) were low (<0.1% for heterotetrapods[17] and <30% for concentric core/shell HNCs[16]). Low PL QYs have been seen as an intrinsic limitation of type-II HNCs,[5] since the slower radiative recombination of indirect excitons can result in the dominance of faster nonradiative processes. However, recent work by a number of groups has demonstrated that the PL QYs of Type-II and Type-I$^{1/2}$ HNCs can be as high as those observed for Type-I HNCs (viz., 50−80% for CdTe/CdSe and CdS/ZnSe HNCs).[3,7,14,15]

Here, we report on the synthesis and optical properties of highly luminescent ultranarrow (~2 nm diameter) (Zn,Cd)Te/CdSe colloidal heteronanowires (Figure 1). The wires are up to

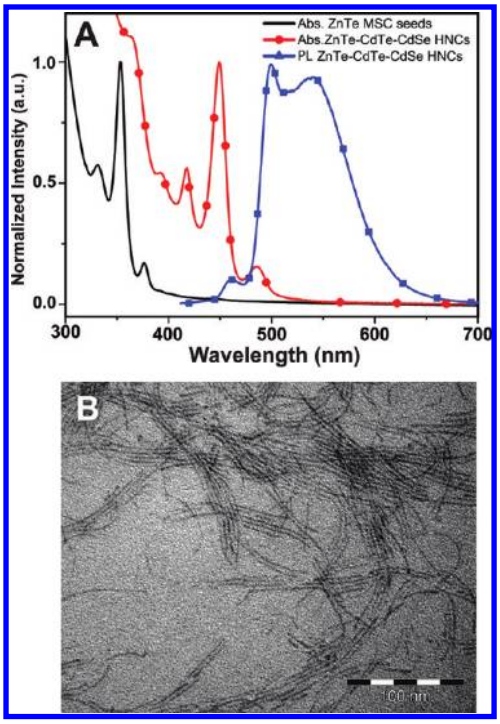

Figure 1. (A) Absorption (Abs) and PL (excitation at 400 nm) spectra of (Zn,Cd)Te/CdSe colloidal heteronanowires obtained by using ZnTe MSCs as seeds. The absorption spectrum of the ZnTe MSC seeds is also shown. (B) Representative TEM image of the (Zn,Cd)Te/CdSe heteronanowire sample used to obtain the spectra shown in (A).

~100 nm long and exhibit high PL QYs (viz., 20−60%). The PL wavelength can be tuned from 530 to 760 nm by controlling the heteronanowire composition, which also strongly influences the exciton lifetimes and the spectral overlap between the absorption and emission (Figure 2). This Letter is organized as follows. First, the mechanism behind the formation of the heteronanowires is addressed. We show that the first step consists of a fast cation exchange, through which Zn is partially replaced by Cd. In the second step, the resulting (Zn,Cd)Te magic size clusters (MSCs) self-organize into segmented heteronanowires. Further growth occurs primarily by inclusion of CdSe between adjoining segments. After establishing the composition and structure of the heteronanowires, we turn to their optical properties. The evolution of the optical properties

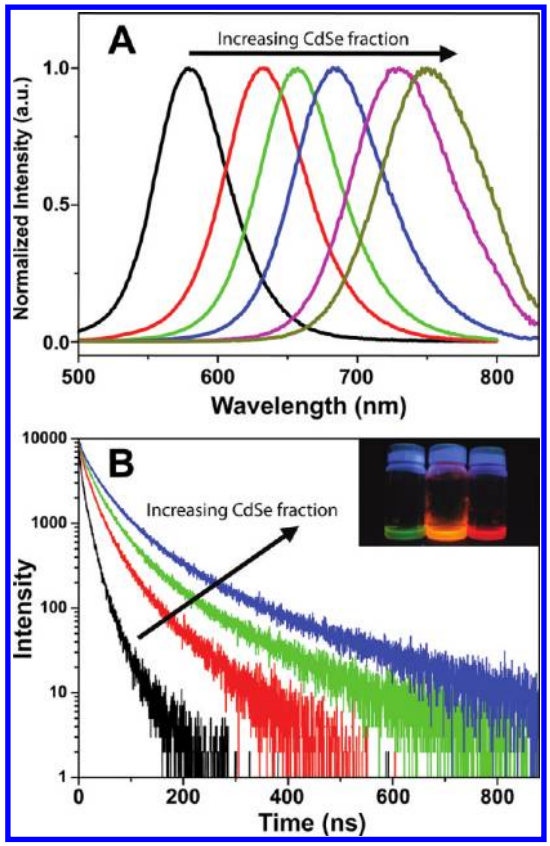

Figure 2. PL spectra (A) and PL decay curves (B) of a series of (Zn,Cd)Te/CdSe colloidal heteronanowires with increasing CdSe volume fraction. The inset in (B) shows some of the (Zn,Cd)Te/CdSe colloidal heteronanowire samples under UV (365 nm) excitation.

during the formation and growth of the heteronanowires clearly indicates that the electron−hole overlap decreases with increasing CdSe volume fraction, shifting all exciton transitions to lower energies and leading to longer exciton lifetimes and smaller spectral overlaps between PL and absorption.

The (Zn,Cd)Te/CdSe heteronanowires are prepared by a multistage seeded growth method in which ZnTe MSCs are used as seeds. In the following, a brief and general description of this method is provided. Full experimental details are given in the Supporting Information.[27−30] In the first stage, ZnTe MSCs are prepared following a recently developed method[27] and isolated from the reaction mixture. The absorption spectrum of a typical sample of ZnTe MSC seeds is given in Figure 1A. The narrow peaks (150 meV) observed in the spectrum are characteristic of MSCs[27] and indicate that the sample consists primarily of ZnTe MSCs with a diameter of 1.5 nm (peak at 354 nm), accompanied by smaller populations of 1.3 and 1.8 nm diameter ZnTe MSCs (peaks at 330 and 378 nm, respectively).[27] These MSCs are characterized by the general formula $[(ZnTe)_n(ZnL_x)_m]$, with $(m + n)/n = 1.4$; L = hexadecylamine, $n \cong 19$, 34, and 48 for MSCs with 1.3, 1.5, and 1.8 nm diameter, respectively.[27] It is worth noting that each MSC family is essentially single-sized, since MSCs contain a well-defined number of atoms arranged in a particularly stable configuration.[27] In the second stage of the heteronanowire synthesis, purified ZnTe MSC seeds are added to a hot (165 °C) coordinating solvent, containing hexadecylamine (HDA), trioctylphosphine (TOP), and the selenium precursor (Se dissolved in TOP). The final stage consists of the dropwise

dx.doi.org/10.1021/nl203695m | Nano Lett. 2012, 12, 749−757

addition of the Cd precursor (anhydrous cadmium acetate in TOP) to the reaction mixture at 165 °C. As an illustrative example, Figure 1 presents the absorption and PL spectra and a representative transmission electron microscopy (TEM) image of the final sample after one Cd addition cycle. The sample consists of narrow wires with a diameter of 2 nm and length ranging from ~20 to ~100 nm.

To investigate whether ZnTe MSCs are required for the heteronanowire formation, syntheses were performed using a mixture of ZnTe MSCs and small NCs as seeds. The absorption spectra of both the seeds and the final HNC sample for a representative synthesis are shown in Figure 3.

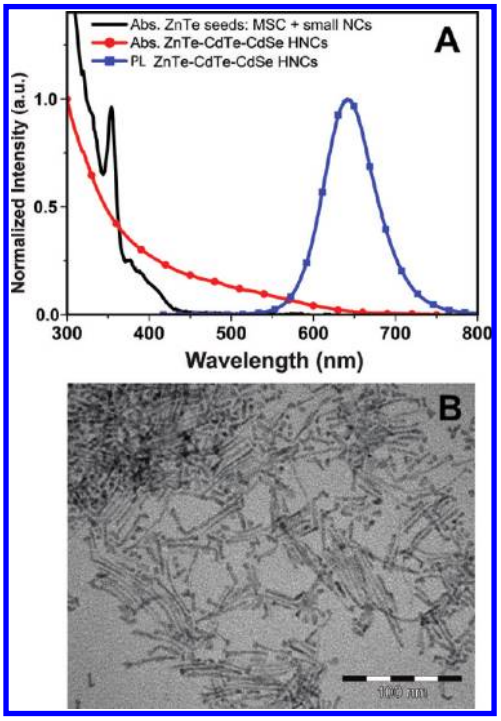

Figure 3. (A) Abs and PL spectra of the (Zn,Cd)Te/CdSe colloidal HNC sample shown in (B). The absorption spectrum of the ZnTe seeds is also given. (B) Representative TEM image of a (Zn,Cd)Te/CdSe heteronanocrystal sample prepared using mixed ZnTe MSCs and small NCs as seeds.

The seeds consist of 1.5 nm ZnTe MSCs (peak at 354 nm) accompanied by a small population of 1.8 nm ZnTe MSCs (peak at 378 nm) and small ZnTe NCs ranging from 2 to 3 nm in diameter (absorption tail from 395 to 420 nm). A pronounced shift of the optical transitions to lower energies takes place upon growth of the HNCs, regardless of the seeds used (Figures 1 and 3). The differences between the absorption and PL spectra of the HNC samples shown in Figures 1 and 3 can be ascribed to the larger CdSe volume fraction and larger shape (and size) distribution of the sample in Figure 3. The relationship between the composition and the optical properties of the HNCs will be discussed in more detail later.

The most striking difference between the syntheses using the two different ZnTe seed populations is observed in the TEM images, which show that HNCs obtained from monodisperse MSC seeds consist of nanowires only (Figure 1B), while nanowires and irregularly shaped "nearly isotropic" HNCs coexist in samples obtained from mixed seeds (Figure 3B). Owing to the different solubilities of the two kinds of HNCs, shape selective precipitation was successfully used to separate them (Supporting Information). Powder X-ray diffraction analysis and TEM images of the two HNC fractions (Supporting Information, Figure S1) show that the "nearly isotropic" HNCs possess the zincblende structure and consist of irregularly shaped pyramids (~4 nm equivalent diameter) and short multipods (~5 nm long, ~2−3 nm diameter pods), while the nanowires have the wurtzite structure and are shorter (~50 nm) and slightly thicker (2.5 nm) than those obtained using monodisperse MSCs as seeds. These results show that the characteristics of the ZnTe NC seeds have a decisive role in the shape and crystal structure of the resulting HNCs. The formation of the irregularly shaped nearly isotropic HNCs can be explained by heteroepitaxial overgrowth on the small NC seeds, while the nanowires clearly require ZnTe MSCs as seeds. This is reflected in the higher quality and longer average length of the nanowires grown from monodisperse ZnTe MSCs as seeds (Figure 1). A possible mechanism for the formation of (Zn,Cd)Te/CdSe heteronanowires from ZnTe MSCs will be proposed below.

High-resolution TEM (HR-TEM) (Figure 4 and Supporting Information, Figure S2) confirms the crystallinity of the nanoparticles and shows that many of the heteronanowires grown using mixed ZnTe seeds contain larger segments that resemble the irregularly shaped nearly isotropic HNCs. In several cases the lattice planes in these segments show a different orientation with respect to the adjoining wire segments. Further, the diameter of the nanowires is not constant throughout their length but oscillates between 1.8 and 2.5 nm, even in the well-formed nanowires obtained from monodisperse ZnTe MSC seeds. It is also clear that the orientation of the fringe patterns varies along the nanowires, sometimes substantially. These observations suggest that the nanowires grow by self-organization of shorter segments into successively longer wires, possibly by oriented attachment. This offers a possible explanation for the imperfections and irregularities in the shape of the nanowires, which are particularly pronounced in the wires grown using the mixture of ZnTe MSCs and small NCs as seeds. Attachment of an irregularly shaped nearly isotropic HNC to a growing nanowire would either disrupt the assembly process, leading to shorter and headed wires, or change the growth direction, leading to malformed wires (L-shaped, Π-shaped, and so forth) with thicker segments. Further, imperfect alignment of the nanowire segments during the attachment could account for the changes observed in the orientation of the fringe patterns along the length of the wires.

Self-organization of smaller NCs by oriented attachment has been proposed to explain the formation of nanowires of a number of different materials.[1] For example, under suitable conditions colloidal CdTe NCs have been observed to spontaneously assemble into CdTe nanowires.[31] Further, the formation of ultranarrow colloidal nanowires (1.3−1.6 nm diameter) from MSCs has been reported for both ZnSe[32] and CdSe.[33,34] The diameter of the nanowire is determined by the parent NC or MSC, while its length depends on the number of attached units and varies widely.[1,31−34] Oriented attachment has also been shown to be involved in the growth of long (>10 nm) CdSe nanorods.[35] To exclude the possibility that the presently observed self-organization is due to drying effects, cryo-TEM measurements were performed on samples obtained using monodisperse ZnTe MSCs as seeds (Supporting Information, Methods). The cryo-TEM images (Supporting

dx.doi.org/10.1021/nl203695m | Nano Lett. 2012, 12, 749−757

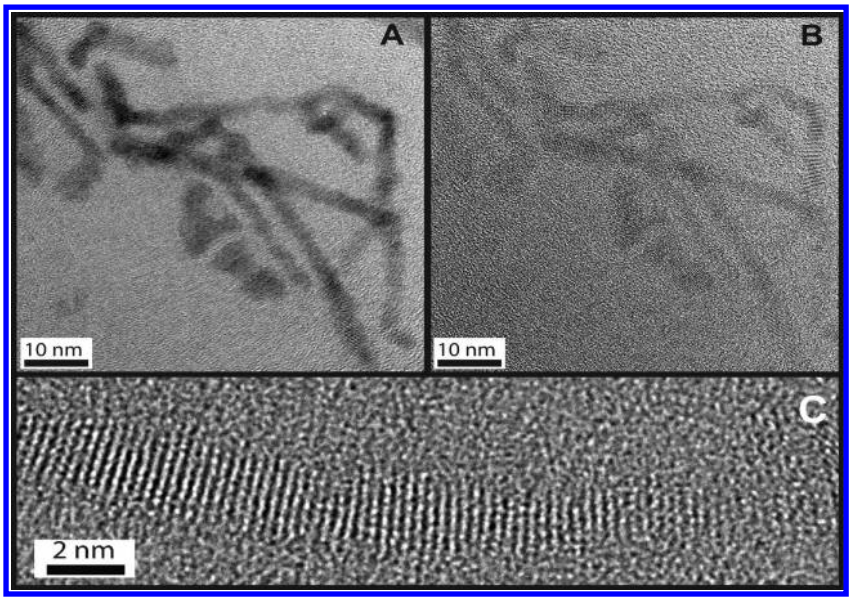

Figure 4. (A,B) HR-TEM image of (Zn,Cd)Te/CdSe heteronanocrystals prepared using mixed ZnTe magic size clusters and small nanocrystals as seeds. (C) HR-TEM image of part of a (Zn,Cd)Te/CdSe heteronanowire showing that the orientation of the lattice fringes changes along the length of the nanowire.

Information, Figure S3a) clearly show stringlike aggregates of short wires (~20 nm long) with equal diameter (~2 nm) and variable lengths. The nanowires degrade quickly under electron beam irradiation (Supporting Information, Figure S3b). It is thus possible that the nanowire fragmentation observed in the cryo-TEM images is partially due to the electron beam irradiation.

Key questions that emerge in the present case are whether the parent units involved in the formation of the hetero-nanowires are already heterostructured, and whether the original ZnTe MSC seeds are preserved in the HNC. To address these questions the composition of the nanowires must be known. Compositional mapping by scanning TEM energy dispersive X-ray spectroscopy (STEM-EDS) failed to provide information on the elemental profile of individual nanowires, since the wires experienced fast degradation upon exposure to the electron beam (Supporting Information, Figure S4). This required the use of low-dose electron beams, which resulted in poor signal-to-noise ratios at the single nanowire level. Therefore, EDS analyses were performed only on wider areas (~10^4–10^5 nm^2), encompassing ~100 to ~1000 HNCs (Figure 5 and Supporting Information Figure S5). The composition of the HNCs was also analyzed by inductively coupled plasma mass spectrometry (ICP-MS). A sample of HNCs obtained from mixed ZnTe seeds (similar to that shown in Figure 3) was also analyzed by scanning TEM electron energy loss spectroscopy (STEM-EELS) (Figure 6). In order to maximize the resolution, only the Cd and Te edges were analyzed, since inclusion of Zn and Se as well would require probing a wider energy window (Supporting Information, Methods).

The elemental concentrations (atom %) determined by EDS for the HNC sample shown in Figure 3 are (45.1 ± 4.3)% for Cd, (9 ± 4)% for Zn, (15.7 ± 0.5)% for Te, and (30.1 ± 2.3)% for Se (average over several observation spots). The Zn content is less reliable for two reasons. First, the Zn and Cu EDS peaks partially overlap (see Figure 5A), which introduces a larger uncertainty in the estimated Zn intensities. Second, the

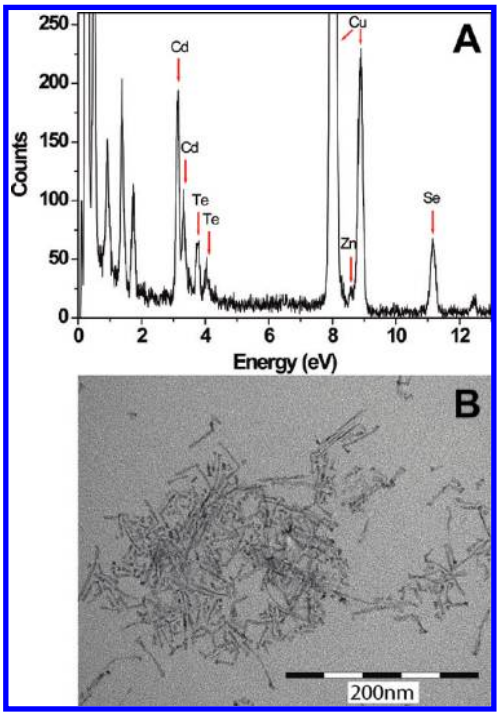

Figure 5. Energy dispersive X-ray spectrum (A) and TEM image (B) of a group of (Zn,Cd)Te/CdSe heteronanocrystals selected for elemental analysis.

variation in the Zn content between different observation spots is much larger than that for the other elements, implying the presence of an additional Zn compound in the samples examined by TEM. Most likely, the additional Zn originates from $Zn(HDA)_x$ complexes formed in the early steps of the nanowire growth (see below). These complexes can only be removed by repeated washing cycles, which also lead to removal of surfactant molecules, causing aggregation and loss of solubility. Therefore, samples for TEM analysis cannot be extensively washed. The loss of solubility is not a problem for

dx.doi.org/10.1021/nl203695m | *Nano Lett.* 2012, 12, 749–757

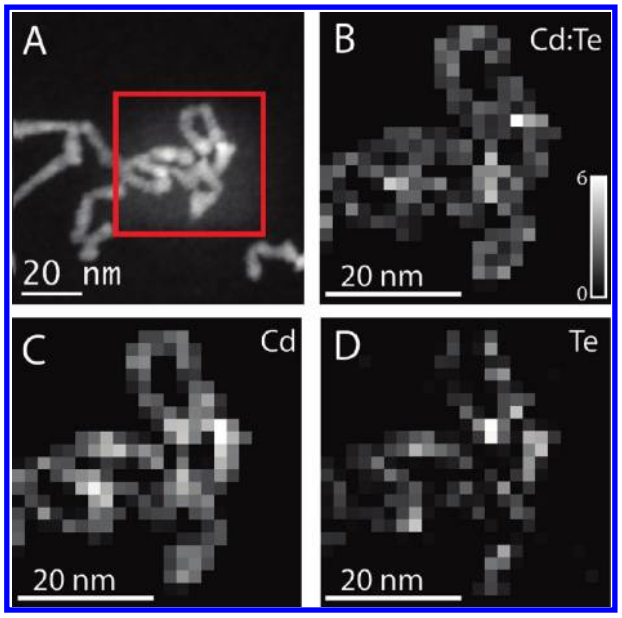

Figure 6. (A) STEM-HAADF image of (Zn,Cd)Te/CdSe heteronanocrystals. The square indicates the region selected for EELS analysis. The Cd/Te elemental ratio map shown in (B) was constructed from the chemical maps for Cd (C) and Te (D).

ICP-MS analysis and therefore samples analyzed by this technique could be thoroughly washed, resulting in more reliable elemental concentration values for Zn.

To allow comparison between the compositions determined by EDS and ICP-MS, it is convenient to express both as elemental ratios relative to the Te content (the element with the smallest standard deviation in the EDS analysis, viz., 3%). The relative elemental ratios for the HNCs shown in Figure 3 are then found to be 0.27 for Zn (taking the smallest value determined), 2.9 ± 0.3 for Cd, and 1.9 ± 0.2 for Se by EDS, and 0.2 for Zn, 2.9 for Cd, and 1.8 for Se by ICP-MS (Te content set to 1.0 in both cases). For the heteronanowire sample shown in Figure 1, the relative elemental ratios are 0.29 for Zn (taking the smallest value determined), 2.3 for Cd, and 1.6 for Se by EDS, and 0.2 for Zn, 2.35 for Cd, and 1.50 for Se by ICP-MS. The agreement between the relative elemental ratios determined by EDS (average over 10^2–10^3 HNCs) and ICP-MS (average over 10^{14}–10^{15} HNCs) is very good, implying that the compositional fluctuations within the HNC ensemble are not very large (<15%).

The Zn/Te ratio of the HNCs is remarkably smaller than that of the parent ZnTe MSCs (viz., 1.42 by ICP-MS), implying that a large fraction of the Zn atoms has been exchanged by Cd atoms prior to or during the process of heteronanowire formation. Given that the metal/chalcogenide ratio of the heteronanowires (viz., 1.02) is also smaller than that of the parent MSCs, one can conclude that 80% of the Zn atoms in the $(ZnTe)_n$ cluster core are exchanged by Cd, while the outer Zn atoms (see general formula for ZnTe MSCs above) are lost to the reaction medium, probably as $Zn(HDA)_x$ complexes. We propose that the Zn for Cd cation exchange reaction occurs prior to the formation of the nanowires, converting the parent ZnTe MSCs into (Zn,Cd)Te MSCs, which subsequently self-organize into nanowires. Further support to this mechanism is given by the observation that nanowires are formed immediately after the addition of Cd precursors, even in the absence of Se precursors (see below).

Cation exchange has recently emerged as a versatile and attractive strategy to fabricate shape-controlled HNCs and NCs that are not attainable by conventional methods[1,36−40] and has successfully yielded a number of novel HNCs (for example, PbSe/CdSe core/shell QDs,[37,40] PbSe/PbS dot core/rod shell heteronanorods,[38] CdSe/CdS hetero-octapods[39]). The common feature in all these synthetic schemes is the utilization of ion exchange reactions to replace the native cationic sublattice with different ions, while preserving the anionic framework.[1,36−39] The cation exchange reactions are driven by the different solubilities of the incoming and outgoing ions and can thus be tuned by choosing suitable solvents and ligands.[36,38,41] The Zn^{2+} by Cd^{2+} place exchange reaction observed here is probably driven by the higher stability of Zn^{2+} complexes with both HDA molecules and acetate anions.[1]

The cation exchange rates have been observed to strongly depend on the particle size. For example, under the same reaction conditions, the Ag^+ for Cd^{2+} exchange has been shown to be virtually absent for micrometer-sized CdSe particles over a period of weeks but to occur in less than a second for 5 nm diameter CdSe NCs and in ∼10 h for 100 nm long CdSe wires.[36] The present observation of Zn^{2+} for Cd^{2+} exchange is thus not surprising considering the extremely small dimensions of the ZnTe MSCs used as seeds (1.3−1.8 nm diameter). However, it is quite remarkable that the exchange reaction does not reach completion in the time scale of our experiments (∼1 h), but instead leads to (Zn,Cd)Te MSCs containing 20 mol % Zn, which corresponds to only a few ZnTe units per (Zn,Cd)Te MSC (viz., ∼ 4, 7, and 10 for the three seed MSC families with 1.3, 1.5, and 1.8 nm diameter, respectively). This observation is in line with earlier studies of ion exchange processes in thiophenolate-capped metal chalcogenide clusters (viz., $[S_4M_{10}(SPh)_{16}]^{4-}$, $[S_4M_{17}(SPh)_{28}]^{2-}$, M = Zn or Cd, Ph = phenyl), which showed that the metal exchange rates decrease for the atoms located toward the center of the clusters, so that the reaction reaches equilibrium before completion.[42] Given that MSCs have very well-defined configurations,[27] all MSCs of a given family are expected to show essentially the same stability and reactivity, and thus similar cation exchange rates. However, different MSC families may show different exchange rates. Therefore, the Zn molar ratios reported here should be regarded as a weighted average between the Zn/Te ratios of all the different MSC families present in the reaction mixture.

The relative volume fractions of CdSe and (Zn,Cd)Te in the heteronanowire samples can be estimated from the elemental composition and the densities of the bulk materials, since the amount of Se is proportional to the fraction of CdSe, and the amount of Te reflects the fraction of (Zn,Cd)Te. This analysis shows that the heteronanowire samples contain similar volumes of CdSe and (Zn,Cd)Te (viz., 55% CdSe, 45% (Zn,Cd)Te; and 60% CdSe, 40% (Zn,Cd)Te, for the samples shown in Figures 1 and 3, respectively). This shows that the nanowires cannot consist of a single (Zn,Cd)Te head from which a long CdSe nanowire grows, since this would lead to much larger CdSe volume fractions. The STEM-EELS measurements (Figure 6) provide valuable insight in the distribution of CdSe and (Zn,Cd)Te at the single heteronanowire level. These measurements were carried out using an EELS spectrum imaging approach,[30] which means that at every pixel of the STEM image (Figure 6A) a full EELS spectrum was recorded (Supporting Information, Methods). From this, element-specific chemical maps were constructed for Cd and Te (Figure 6C,D, respectively), which clearly show that Cd and Te are distributed

dx.doi.org/10.1021/nl203695m | Nano Lett. 2012, 12, 749−757

throughout the HNCs and are present in all HNCs. Moreover, the Cd/Te elemental ratio map (Figure 6B) shows that the Cd to Te ratio is not homogeneous throughout the HNCs but instead exhibit modulations on a length scale of the order of the pixel size (~2 × 2 nm^2). These observations rule out that the wires consist of a (Zn,Cd)(Te,Se) homogeneous alloy or that (Zn,Cd)Te-rich and CdSe-rich nanowires coexist in the same sample. This provides strong evidence that the nanowires are formed by assembly of (Zn,Cd)Te/CdSe segments that are heterostructured on a length scale of the order of 2−10 nm. As will be discussed later, this is consistent with the optical properties of the HNCs. However, the dimensions (both diameter and length) of the individual (Zn,Cd)Te and CdSe domains and the way they are organized within the various segments remain to be elucidated. For instance, it is possible that CdSe occurs both as single composition domains collinearly connected to (Zn,Cd)Te domains and as shells (partially) overcoating (Zn,Cd)Te sections of the nanowire. Nevertheless, our observations do not allow any quantitative conclusion in this respect. Moreover, the present results are also inconclusive regarding the compositional profile of the (Zn,Cd)Te domains of the heterosegments, and it is as yet unclear whether they can be regarded as ZnTe/CdTe core/shell HNCs or (Zn,Cd)Te alloy NCs.

It is noteworthy that no spectral changes are observed after mixing the Se precursor and the ZnTe MSC seeds at the reaction conditions. It is only after the addition of the Cd precursor that pronounced spectral changes take place (viz., appearance of PL and shift of the optical transitions to lower energies). To investigate the role of TOP-Se, a synthesis was performed in the absence of Se precursors, while keeping the Cd addition rates and other reaction conditions unchanged. Samples were collected 90 s and 10 min after Cd addition. Despite the absence of the Se precursor, the Cd addition immediately led to the appearance of PL and induced a pronounced shift of the optical transitions to lower energies (Figure 7). Interestingly, the samples collected also consist of nanowires (Figure 7B) with dimensions similar to those of the (Zn,Cd)Te/CdSe heteronanowires obtained in the presence of Se precursors (see above). The metal to Te ratio was found by ICP-MS to be 0.1 for Zn and 0.9 for Cd for the 90 s sample and 0.1 for Zn and 1.0 for Cd for the 10 min sample. This shows that the Zn^{2+} for Cd^{2+} place exchange reaction is very fast, reaching equilibrium already before 90 s. Further, as observed for the (Zn,Cd)Te/CdSe heteronanowires, the exchange is not complete but reaches equilibrium for Te/Zn = 0.1. It is as yet unclear whether the differences between the equilibrium Zn content in the two syntheses reflect a synergistic interaction with the Se precursor or are simply due to experimental uncertainties (for example, reaction temperature, concentrations, and so forth). To check whether Se can be incorporated at later reaction stages, Se precursor was added to the reaction mixture ~10 min after the addition of the Cd precursor. This led to a further shift of all the optical transitions to lower energies. The incorporation of CdSe is clearly evident from the elemental composition of the heteronanowires (viz., Cd, 3.2; Zn, 0.1; Te, 1; Se, 1.85, by ICP-MS). It is interesting to note that the Te/Zn ratio remains constant, showing that Te for Se exchange does not occur.

The results presented above clearly establish that the first step in the formation of the colloidal heteronanowires prepared in this work consists of a fast Zn^{2+} for Cd^{2+} place exchange that converts the parent ZnTe MSCs into (Zn,Cd)Te MSCs while

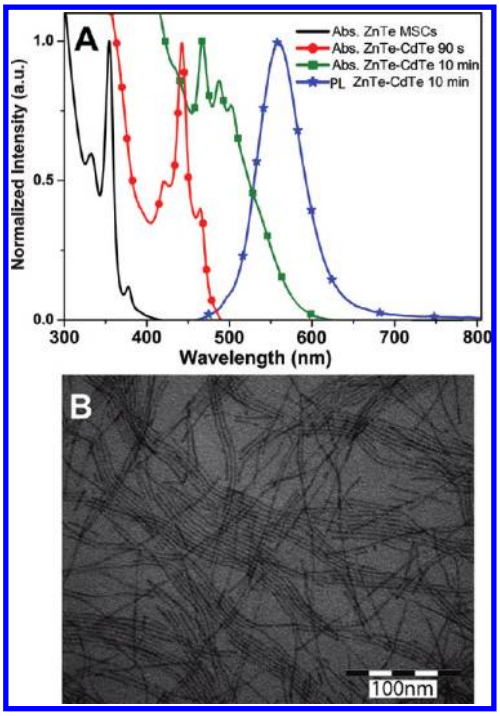

Figure 7. (A) Abs spectra of (Zn,Cd)Te colloidal heteronanowire samples collected 90 s and 10 min after Cd addition to ZnTe MSC seeds. The absorption spectrum of the ZnTe MSC seeds is also shown. For clarity, only the PL spectrum of the 10 min sample is shown, although the 90 s sample already displayed PL (peak at 500 nm). (B) Representative TEM image of a (Zn,Cd)Te heteronanowire sample collected 10 min after the addition of Cd precursor to ZnTe MSC seeds.

preserving the cluster configuration. The (Zn,Cd)Te MSCs self-organize into strings, which subsequently undergo fusion-forming segmented nanowires. Considering that both (Zn,Cd)Te and (Zn,Cd)Te/CdSe heteronanowires are obtained, it is clear that Se is not required for the nanowire formation. This implies that the ability to self-organize into nanowires is inherent to the (Zn,Cd)Te MSCs. The driving force for this self-organization process remains to be elucidated. It is generally accepted that self-organization by oriented attachment is driven by dipolar interactions between the parent units, even though in most cases the origin of these putative dipole moments remains unclear.[1] In the present case, the dipolar interactions could be the result of an asymmetry in the distribution of disparate ligands (long and neutral HDA versus small and charged acetate molecules) among the binding sites in the (Zn,Cd)Te MSCs. It is also possible that the linear HDA molecules have an adjuvant role, facilitating the self-assembly into strings. Further growth of the nanowire occurs by incorporation of CdSe, which can occur both by growth of collinear domains inserted between adjoining segments (since the junctions between segments should be highly dynamic) and by overcoating of sections of the nanowire. This process results into segmented nanowires, in which the segments are heterostructured on short length scales with (Zn,Cd)Te and CdSe domains of the order of 2−10 nm.

The heterostructured nature of the colloidal heteronanowires prepared in this work is clearly reflected in their optical properties. The (Zn,Cd)Te/CdSe (Figures 1−3) and (Zn,Cd)Te (Figure 7) nanowires are both highly luminescent, in striking contrast to the parent ZnTe MSCs. Reports on the

dx.doi.org/10.1021/nl203695m | *Nano Lett.* 2012, 12, 749−757

luminescence of colloidal ZnTe NCs are scarce, possibly because the high-energy position of the band edges of ZnTe makes it difficult to efficiently passivate the surface atoms, since most ligands have energy levels below the band edges of (bulk) ZnTe.[27] This explains why in the present case PL appears immediately after the first Cd addition, reflecting the transformation from a Zn-terminated to a primarily Cd-terminated surface. The PL QYs of the heteronanowires are remarkably high (viz., 20−60%), especially considering their large surface to volume ratio and heterostructured nature. Such high PL QYs indicate relatively slow nonradiative recombination rates, implying low defect concentrations and attesting the high-quality of the heteronanowires prepared by the presently reported method.

The PL of the (Zn,Cd)Te/CdSe heteronanowires can be tuned from 530 to 760 nm by increasing the CdSe volume fraction (Figures 1 and 2). The shift of the emission transition to lower energies is accompanied by an increase of the exciton lifetimes (viz., from ∼20 to 700 ns). The PL decay curves are multiexponential (see, for example, Figure 2) and can be adequately described by a three-exponential fit (Supporting Information, Figures S6 and S7). The exciton radiative lifetime (W_{RAD}) is taken to be equal to the longest component. The multiexponential character of the PL decay can be ascribed to a combination of factors. First, nonradiative recombination probably contributes to the decay rates at early times, since the PL QYs are nonunity, albeit high. Second, the segmented and heterostructured nature of the nanowires gives rise to an intrananowire energy transfer (ET) process, through which the exciton is transferred from segments with larger energy gaps to segments with smaller energy gaps. At earlier times the decay transients are thus dominated by the donor segments of the nanowires, which decay with a faster rate (viz., $W_{RAD} + W_{ET}$). At longer times, only the acceptor nanowire segments with efficient PL (that is, negligible W_{NRAD}) are observed.

In this context, it is interesting to note that the PL wavelength and the exciton radiative lifetimes of the differently shaped (Zn,Cd)Te/CdSe HNCs obtained in the synthesis using mixed ZnTe MSCs and NCs as seeds (viz., heteronanowires and "nearly isotropic" HNCs, see above) are the same, despite the differences in shape and crystal structure (Supporting Information, Figure S8). This observation strongly supports the occurrence of intrananowire ET processes in the (Zn,Cd)Te/CdSe heteronanowires investigated here. As discussed above, nearly isotropic HNCs are incorporated in the heteronanowires during their assembly process when mixed ZnTe MSCs and NCs are used as seeds. Since the nearly isotropic HNCs are larger than the adjoining heteronanowire segments, they will function as energy acceptor segments after the photoexcitation, thereby dominating the exciton radiative recombination. This intrananowire ET process is expected to occur also in regular heteronanowires, such as those shown in Figure 1, since they consist of random assemblies of heterostructured segments. Segments that are richer in CdSe (for being slightly longer and/or thicker) will have smaller energy gaps (see discussion below) and will thus function as acceptor segments. ET processes have been extensively investigated in QD solids and are usually assumed to be mediated by dipole−dipole interactions.[43,44] ET by exchange interaction is usually neglected for QD solids since it requires very small donor−acceptor distances.[44] In the present case, both mechanisms may be active, since the heteronanowire segments are in direct contact.

The evolution of the optical properties of the (Zn,Cd)Te/CdSe heteronanowires as a function of their composition follows the same overall trend previously observed for CdTe/CdSe HNCs.[7] The increase in the CdSe volume fraction results in a progressive shift of all optical transitions to lower energies, accompanied by a decrease of the oscillator strengths at emission energies and an increase of the exciton radiative lifetimes. The radiative exciton lifetimes become longer than those of CdTe or CdSe QDs emitting at similar wavelengths (viz., 15−60 ns in the 2.3−1.75 eV range[45]). For example, the exciton radiative lifetime observed for the (Zn,Cd)Te/CdSe heteronanowire sample shown in Figure 2 with PL peak at 750 nm is 1 order of magnitude longer than that of a CdTe QD emitting at similar energies (Supporting Information, Figure S7). These observations indicate that the overlap between the electron and hole wave functions decreases as the CdSe volume fraction in the (Zn,Cd)Te/CdSe heteronanowires increases, as a result of an increasingly larger spatial separation. In the CdTe/CdSe system, it has been demonstrated that the hole localizes in the CdTe part of the HNC already for small CdSe volume fractions, so that the evolution of the optical properties is primarily determined by the localization regime of the electron.[7] The electron wave function is initially delocalized over the whole HNC and gradually localizes in the CdSe part as its volume fraction increases. In the present system, a similar situation is expected with the hole localized in the (Zn,Cd)Te domains because the bulk valence band potentials of ZnTe and CdTe are essentially the same.[1] (Zn,Cd)Te homogeneous alloys behave as single composition materials with band potentials intermediate to those of ZnTe and CdTe, while the offset between the conduction bands of bulk ZnTe and CdTe is such that the electron localizes in CdTe.[1] Therefore, it can be expected that the electron localization in the CdSe domains of the heteronanowires will be facilitated in the (Zn,Cd)Te/CdSe system, regardless of whether the (Zn,Cd)Te domains behave electronically as ZnTe/CdTe core/shell or (Zn,Cd)Te alloy NCs.

The onset of the type-II localization regime has been shown to be characterized by the loss of structure of the lowest energy absorption band, accompanied by a simultaneous increase in the Stokes shift values and transition linewidths.[7] On the basis of these spectral signatures, we can conclude that in the present system the type-II regime is achieved only for the final samples of the synthesis using mixed ZnTe MSCs and NCs as seeds (see, for example, Figure 3). The (Zn,Cd)Te/CdSe heteronanowires obtained by using only ZnTe MSCs as seeds (see, for example, Figure 1) are still in the Type-$I^{1/2}$ localization regime, as clearly evidenced by the narrow peaks, absence of Stokes shift and reasonably short exciton lifetime (viz., 46 ns, Supporting Information, Figure S6a). The emission spectrum of this sample consists of a combination of narrow peaks and a broad band (Figure 1). The narrow peaks are resonant with the lowest two peaks in the absorption spectrum and can thus be ascribed to the recombination of a direct exciton (type-$I^{1/2}$ regime) in two types of heteronanowires (or segments thereof) that differ slightly in composition and/or diameter. The excitation spectra of the broad PL band and of the lowest energy narrow PL peak are the same, indicating that the two emitting states share a common excitation channel. This may be attributed to an intrananowire energy transfer process involving segments with different degrees of electron−hole overlap with the broad band originating from the segment with the larger degree of spatial separation.

dx.doi.org/10.1021/nl203695m | Nano Lett. 2012, 12, 749−757

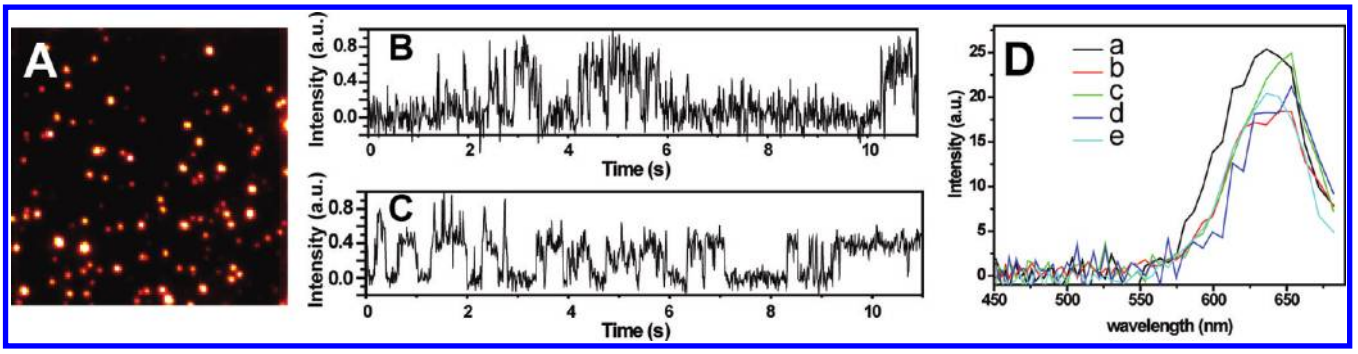

Figure 8. (A) PL microscopy image of a diluted ensemble of (Zn,Cd)Te/CdSe heteronanocrystals spin-coated on a glass surface (128 × 128 pixels, 1 pixel = 182 nm). The image is an integrated stack of 1000 single frames (10 ms exposure/frame). A stream of 200 frames is shown in the Supporting Information (Movie S1). The heteronanocrystals clearly display fluorescence intermittency. Representative PL time traces for selected regions are depicted in (B) and (C). (D) PL spectra of selected regions.

Interestingly, the absorption spectrum of the heteronanowires obtained by using only ZnTe MSCs as seeds (Figure 1A) is very similar to that of the parent MSCs, despite a ~750 meV shift to lower energies. As discussed above, this large shift in the transition energies is due to the dramatic change in composition that results from the conversion of ZnTe MSCs to $(Zn_{0.2}Cd_{0.8})Te/(CdSe)_{1.5}$ heteronanowires. The bandwidth of the absorption peaks is even narrower (95 meV) than that of the parent ZnTe MSCs (150 meV). Considering that the exciton transition energies in quantum confined systems are strongly dependent on the composition and size of the nanostructure,[1] the observation of such narrow linewidths for an ensemble of nanowires in the strong quantum confinement regime (exciton Bohr radii are 7.3 and 4.9 nm for CdTe and CdSe, respectively[45]) implies a narrow distribution in the diameter and composition of the heteronanowire segments. The observation of three narrow peaks is consistent with the fact that the parent ZnTe MSCs consisted of three different families, implying that only three well-defined families of (Zn,Cd)Te MSCs were obtained after the Zn^{2+} for Cd^{2+} place exchange reaction.

To further investigate the degree of compositional homogeneity within an ensemble of (Zn,Cd)Te/CdSe heteronanowires, the PL spectra of a number of individual nanowires were measured at room temperature (Supporting Information, Methods). A detailed discussion of the single heteronanowire PL spectra lies beyond the scope of this Letter and will be presented elsewhere. Here we will focus on the extent to which these measurements provide information over the compositional distribution within the HNC ensemble. The heteronanowires clearly display fluorescence intermittency ("on–off" behavior or blinking) (Figure 8 and Supporting Information, Figure S9 and Movie S1). Although the fluorescence intermittency mechanism is still not fully understood, it is well established that blinking provides unequivocal evidence that the observed emission originates from a single fluorophore.[46–48] The PL spectra of a number of single heteronanowires are shown in Figure 8. It is clear that the spectral distributions for all the observed heteronanowires are similar. This is remarkable and can be understood by considering that each nanowire consists of a large number of (Zn,Cd)Te/CdSe heterostructured segments. Given that the segments are not identical, each nanowire can be seen as a collection of single fluorophores. Because the number of segments per nanowire is large in comparison to the distribution of energy gaps of the available building segments, each heteronanowire will likely contain a sufficiently large diversity of emitting domains to reflect the ensemble distribution. Therefore, the time-integrated PL peak of a single heteronanowire will be close to the ensemble average.

In conclusion, we presented a facile synthetic approach to prepare ultranarrow (Zn,Cd)Te/CdSe and (Zn,Cd)Te colloidal segmented heteronanowires with ~2 nm in diameter and up to 100 nm long. The utilization of ZnTe MSCs as seeds is shown to be essential for the heteronanowire formation. The first step in the formation mechanism consists of a fast cation exchange, through which Zn atoms are partially replaced by Cd. In the second step, the resulting (Zn,Cd)Te MSCs self-organize into segmented nanowires. Further growth of the heteronanowire occurs by inclusion and/or deposition of CdSe. The wires are highly luminescent and emit in the 530 to 760 nm range. The optical properties can be controlled by adjusting the nanowire composition. The results show that by increasing the CdSe volume fraction of the heteronanowires the electron–hole overlap is reduced, leading to longer exciton lifetimes and smaller spectral overlaps between PL and absorption, and shifting all exciton transitions to lower energies. Semiconductor nanowires hold great promise for applications in photovoltaics, solid-state lighting, solar energy conversion, and photonics.[49–51] The colloidal heteronanowires reported here are potentially interesting as active elements in light harvesting and photovoltaic devices, since the combination of large surface to volume ratio and partial electron–hole spatial separation may greatly facilitate carrier extraction. In addition, this work raises a number of interesting issues that merit further investigation. First, the exact compositional and structural profiles of the heteronanowires have yet to be unraveled. Further, the extent to which the different nanowire segments are electronically coupled remains to be elucidated. Moreover, the impact of the combined effects of shape anisotropy, wire segmentation, strong quantum confinement, and (partial) carrier separation on a number of properties (for example, Auger recombination, carrier and spin relaxation rates, emission polarization, and so forth) has yet to be evaluated.

■ ASSOCIATED CONTENT

Ⓢ Supporting Information

Detailed experimental methods and figures showing HR-TEM images, XRD diagrams, and PL spectra of differently shaped heteronanocrystals, Cryo-TEM images, degradation of heteronanowires due to electron beam irradiation, TEM-EDS analyses, and PL decay curves of the heteronanowires. A

dx.doi.org/10.1021/nl203695m | Nano Lett. 2012, 12, 749–757

movie showing the photoluminescence intermittency of single heteronanowires is also provided. This material is available free of charge via the Internet at http://pubs.acs.org.

AUTHOR INFORMATION

Corresponding Author

*E-mail: (C.d.M.D.) c.demello-donega@uu.nl; (E.G.) e.groeneveld@uu.nl.

ACKNOWLEDGMENTS

The authors are grateful to K. Lambert and Z. Hens (Physics and Chemistry of Nanostructures, Ghent University, Belgium) for HRTEM measurements and to O. Stephan (Laboratoire de Physique des Solides, Université Paris Sud XI, France) for assistance regarding the STEM-EELS measurements. M.M.vS and A.G. acknowledge financial support from the 13 European project ESTEEM (No. 026019).

REFERENCES

(1) Donega, C. d. M. *Chem. Soc. Rev.* **2011**, *40*, 1512−1546.
(2) Reiss, P.; Protière, M.; Li, L. *Small* **2009**, *5*, 154−168.
(3) Ivanov, S. A.; Piryatinski, A.; Nanda, J.; Tretiak, S.; Zavadil, K. R.; Wallace, W. O.; Werder, D.; Klimov, V. I. *J. Am. Chem. Soc.* **2007**, *129*, 11708−11719.
(4) Pandey, A.; Guyot-Sionnest, P. *Science* **2008**, *322*, 929−932.
(5) Lo, S. S.; Mirkovic, T.; Chuang, C.; Burda, C.; Scholes, G. D. *Adv. Mater.* **2011**, *23*, 180−197.
(6) Oron, D.; Kazes, M.; Banin, U. *Phys. Rev. B* **2007**, *75*, 035330.
(7) Donega, C. d. M. *Phys. Rev. B* **2010**, *81*, 165303.
(8) Brovelli, S.; Schaller, R. D.; Crooker, S. A.; Garcia-Santamaria, F.; Chen, Y.; Viswanatha, R.; Hollingsworth, J. A.; Htoon, H.; Klimov, V. I. *Nat. Comm.* **2011**, *2*, 280.
(9) Kim, S.; Fisher, B.; Eisler, H.-J.; Bawendi, M. G. *J. Am. Chem. Soc.* **2003**, *125*, 11466−11467.
(10) Halpert, J. E.; Porter, V. J.; Zimmer, J. P.; Bawendi, M. G. *J. Am. Chem. Soc.* **2006**, *128*, 12590−12591.
(11) Zhong, H.; Scholes, G. D. *J. Am. Chem. Soc.* **2009**, *131*, 9170−9171.
(12) Fiore, A.; Mastria, R.; Lupo, M. G.; Lanzani, G.; Giannini, C.; Carlino, E.; Morello, G.; De Giorgi, M.; Li, Y.; Cingolani, R.; Manna, L. *J. Am. Chem. Soc.* **2009**, *131*, 2274−2282.
(13) Koo, B.; Korgel, B. A. *Nano Lett.* **2008**, *8*, 2490−2496.
(14) Zhang, W.; Chen, G.; Wang, J.; Ye, B.-C.; Zhong, X. *Inorg. Chem.* **2009**, *48*, 9723−9731.
(15) Chin, P. T. K.; Donega, C. d. M.; van Bavel, S. S.; Meskers, S. C. J.; Sommerdijk, N. A. J. M.; Janssen, R. A. J. *J. Am. Chem. Soc.* **2007**, *129*, 14880−14886.
(16) Xie, R.; Zhong, X.; Basché, T. *Adv. Mater.* **2005**, *17*, 2741−2745.
(17) Xie, R.; Kolb, U.; Basché, T. *Small* **2006**, *2*, 1454−1457.
(18) Bang, J.; Park, J.; Lee, J. H.; Won, N.; Nam, J.; Lim, J.; Chang, B. Y.; Lee, H. J.; Chon, B.; Shin, J.; Park, J. B.; Choi, J. H.; Cho, K.; Park, S. M.; Joo, T.; Kim, S. *Chem. Mater.* **2010**, *22*, 233−240.
(19) Hewa-Kasakarage, N. N.; El-Khoury, P. Z.; Tarnovsky, A. N.; Kirsanova, M.; Nemitz, I.; Nemchinov, A.; Zamkov, M. *ACS Nano* **2010**, *4*, 1837−1844.
(20) Acharya, K. P.; Khnayzer, R. S.; O'Connor, T.; Diederich, G.; Kirsanova, M.; Klinkova, A.; Roth, D.; Kinder, E.; Imboden, M.; Zamkov, M. *Nano Lett.* **2011**, *11*, 2919−2926.
(21) Sitt, A.; Salant, A.; Menagen, G.; Banin, U. *Nano Lett.* **2011**, *11*, 2054−2060.
(22) Choi, C. L.; Li, H.; Olson, A. C. K.; Jain, P. K.; Sivasankar, S.; Alivisatos, A. P. *Nano Lett.* **2011**, *11*, 2358−2362.
(23) van de Walle, D. C. G.; Neugebauer, J. *Nature* **2003**, *423*, 626.
(24) Tsai, M. H.; Peiris, F. C.; Lee, S.; Furdyna, J. K. *Phys. Rev. B* **2002**, *65*, 235202.
(25) Santangelo, S. A.; Hinds, E. A.; Vlaskin, V. A.; Archer, P. I.; Gamelin, D. R. *J. Am. Chem. Soc.* **2007**, *129*, 3973−3978.
(26) Sellers, I. R.; Whiteside, V. R.; Kuskovsky, I. L.; Govorov, A. O.; McCombe, B. D. *Phys. Rev. Lett.* **2008**, *100*, 136405.
(27) Groeneveld, E.; van Berkum, S.; Meijerink, A.; Donegá, C. d. M. *Small* **2011**, *7*, 1247−1256.
(28) Donega, C. d. M.; Hickey, S. G.; Wuister, S. F.; Vanmaekelbergh, D; Meijerink, A. *J. Phys. Chem. B* **2003**, *107*, 489−496.
(29) Donega, C. d. M.; Bode, M.; Meijerink, A. *Phys. Rev. B* **2006**, *74*, 085320.
(30) van Schooneveld, M. M.; Gloter, A.; Stephan, O.; Zagonel, L. F.; Koole, R.; Meijerink, A.; Mulder, W. J. M.; de Groot, F. M. F. *Nat. Nanotechnol* **2010**, *5*, 538−544.
(31) Tang, Z.; Kotov, N. A.; Giersig, M. *Science* **2002**, *297*, 237−240.
(32) Panda, A. B.; Acharya, S.; Efrima, S. *Adv. Mater.* **2005**, *17*, 2471.
(33) Riehle, F. S.; Bienert, R.; Thomann, R.; Urban, G. A.; Krüger, M. *Nano Lett.* **2009**, *9*, 514−518.
(34) Pradhan, N.; Xu, H.; Peng, X. *Nano Lett.* **2006**, *6*, 720−724.
(35) Yu, Z.; Hahn, M. A.; Maccagnano-Zacher, S. E.; Calcines, J.; Krauss, T. D.; Alldredge, E. S.; Silcox, J. *ACS Nano* **2008**, *2*, 1179−1188.
(36) Son, D. H.; Hughes, S. M.; Yin, Y.; Alivisatos, A. P. *Science* **2004**, *306*, 1009−1012.
(37) Pietryga, J. M.; Werder, D. J.; Williams, D. J.; Casson, J. L.; Schaller, R. D.; Klimov, V. I.; Hollingsworth, J. A. *J. Am. Chem. Soc.* **2008**, *130*, 4879−4885.
(38) Jain, P. K.; Amirav, L.; Aloni, S.; Alivisatos, A. P. *J. Am. Chem. Soc.* **2010**, *132*, 9997−9999.
(39) Deka, S.; Miszta, K.; Dorfs, D.; Genovese, A.; Bertoni, G.; Manna, L. *Nano Lett.* **2010**, *10*, 3770−3776.
(40) Grodzinska, D.; Pietra, F.; van Huis, M. A.; Vanmaekelbergh, D.; Donega, C. d. M. *J. Mater. Chem.* **2011**, *21*, 11556−11565.
(41) Luther, J. M.; Zheng, H.; Sadtler, B.; Alivisatos, A. P. *J. Am. Chem. Soc.* **2009**, *131*, 16851−16857.
(42) Lover, T.; Henderson, W.; Bowmaker, G. A.; Seakins, J. M.; Cooney, R. P. *Inorg. Chem.* **1997**, *36*, 3711−3723.
(43) Wuister, S. F.; Koole, R.; Donega, C. d. M.; Meijerink, A. *J. Phys. Chem. B* **2005**, *109*, 5504−5508.
(44) Rogach, A. L.; Klar, T. A.; Lupton, J. M.; Meijerink, A.; Feldmann, J. *J. Mater. Chem.* **2009**, *19*, 1208−1221.
(45) Donega, C. d. M.; Koole, R. *J. Phys. Chem. C* **2009**, *113*, 6511−6520.
(46) van Sark, W. G. J. H. M.; Frederix, P. L. T. M.; van den Heuvel, D. J.; Gerritsen, H. C.; Bol, A. A.; van Lingen, J. N. J.; Donega, C. d. M.; Meijerink, A. *J. Phys. Chem. B* **2001**, *105*, 8281−8284.
(47) Wang, X.; Ren, X.; Kahen, K.; Hahn, M. A.; Rajeswaran, M.; Maccagnano-Zacher, S.; Silcox, J.; Cragg, G. E.; Efros, A. L.; Krauss, T. D. *Nature* **2009**, *459*, 686−689.
(48) Zhao, J.; Nair, G.; Fisher, B. R.; Bawendi, M. G. *Phys. Rev. Lett.* **2010**, *104*, 157403.
(49) Tian, B.; Kempa, T. J.; Lieber, C. M. *Chem. Soc. Rev.* **2009**, *38*, 16−24.
(50) Yan, R.; Gargas, D.; Yang, P. *Nat. Photonics* **2009**, *3*, 569−576.
(51) Hochbaun, A. I.; Yang, P. *Chem. Rev.* **2010**, *110*, 527−546.